Food Chemistry 394 (2022) 133517

Contents lists available at ScienceDirect

Food Chemistry

journal homepage: www.elsevier.com/locate/foodchem

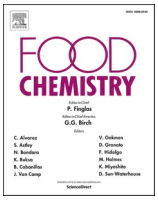

Branched poly(ethylenimine) carbon dots-MnO_2 nanosheets based fluorescent sensory system for sensing of malachite green in fish samples

Xiaowei Mu [a], Xin Liu [a], Xiwen Ye [a], Wei Zhang [a], Lu Li [b,*], Pinyi Ma [a,*], Daqian Song [a,*]

[a] Jilin Province Research Center for Engineering and Technology of Spectral Analytical Instruments, College of Chemistry, Jilin University, Qianjin Street 2699, Changchun 130012, China
[b] State Key Laboratory of Inorganic Synthesis and Preparative Chemistry, College of Chemistry, Jilin University, Qianjin Street 2699, Changchun 130012, China

ARTICLE INFO

Keywords:
Malachite green
Butyrylcholinesterase
Carbon dots
Forster resonance energy transfer

ABSTRACT

Malachite green (MG) is an organic dye compound that is frequently used as a fungicide and antiseptic in aquaculture. However, human or animal exposure to MG causes carcinogenic, teratogenic and mutagenic effects. Herein, a novel fluorescent assay was designed for the detection of MG using manganese dioxide nanosheets (MnO_2 NS) as an energy acceptor to quench the fluorescence of branched poly(ethylenimine) carbon dots (BPEI-CDs) via Förster resonance energy transfer. When butyrylcholinesterase is introduced to form thiocholine in the presence of S-butyrylthiocholine iodide, MnO_2 NS can be recovered by thiocholine to Mn^{2+}, resulting in restoration of the fluorescence of BPEI-CDs. Exploiting these changes in fluorescence intensity in the above system, a fluorescence probe was successfully developed for the quantitative detection of MG. Besides, this assay was applied to fish samples, verifying the high potential for practical application of the proposed sensor for the monitoring of MG in aquatic products.

1. Introduction

Malachite green (MG) is a synthetic triphenylmethane compound that has been widely used as a dye in the paper, textile and leather industries and as a biological stain for cells and tissues (Alderman, 1985). Furthermore, due to its capacity to kill bacteria, fungi and parasites, MG can be used in fisheries to allow the transport of aquatic products and disinfect water tanks, and to treat various fish diseases (Foster & Woodbury, 1936; Leteux & Meyer, 1972). However, after MG enters the body of aquatic animals it becomes a fat-soluble substance and bioaccumulates, with the potential to be transferred to humans via the food chain (Stammati, Nebbia, Angelis, Albo, Carletti, Rebecchi, et al., 2005). With social development and the increasing diversity of food products available worldwide, food safety has become a major global issue (da Cunha, 2021; Nyarugwe, Linnemann, Hofstede, Fogliano, & Luning, 2016). Research has shown that MG and its metabolites are metabolized more slowly in fatty fish and tissues (Fallah & Barani, 2014; Jiang, Xie, & Liang, 2009). In addition, MG can cause chronic toxicity and genotoxicity to mammals and humans through the food chain and has three potential risks (teratogenic, carcinogenic, and mutagenic) (Mittelstaedt, Mei, Webb, Shaddock, Dobrovolsky, McGarrity, et al., 2004; Srivastava, Sinha, & Roy, 2004). Furthermore, due to the slow metabolism and degradation of MG in the environment, the use of MG results in the pollution of water resources (Khan, Otero, Kazi, Alqadami, Wabaidur, Siddiqui, et al., 2019; Samiey & Toosi, 2010). The United States, Canada, China, and many other countries have listed MG as a banned substance for aquaculture, specifying that it must not be detectable in animal foodstuff or aquatic products. However, no low-cost and effective substitutes for MG are available and the current detection methods are high cost, resulting in the ongoing illegal use of MG worldwide. Therefore, the development of simple, rapid and sensitive methods for the detection of MG is essential for food safety and environmental science (Zhou, Zhang, Pan, & Li, 2019).

So far, there have been studies on the detection of MG residues in natural water bodies, aquatic products, starch products, tea and fish feed (Aydin, Yilmaz, & Soylak, 2017; Gavrilenko, Volgina, Pugachev, & Gavrilenko, 2019; Li, Yang, Qi, Qiao, & Deng, 2008). Some methods have been developed for MG detection, including surface-enhanced Raman scattering (SERS) (Deng, Lin, Li, Huang, Kuang, Chen, et al., 2019; Xu, Guo, Huang, Li, & Sun, 2018), electrochemical analysis (Sacara, Cristea, & Muresan, 2017; Lidong Wu, Xu, Meng, Xiao, Cao, Rathi, et al., 2020), high-performance liquid chromatography (HPLC) (Xie, Peng, Chen, Zhang, Wang, Wang, et al., 2013), the enzyme-linked immunosorbent assay (ELISA) (Li, Peng, Lin, Zhong, Chen, & Huang,

* Corresponding authors.
E-mail addresses: luli@jlu.edu.cn (L. Li), mapinyi@jlu.edu.cn (P. Ma), songdq@jlu.edu.cn (D. Song).

https://doi.org/10.1016/j.foodchem.2022.133517
Received 20 October 2021; Received in revised form 11 May 2022; Accepted 16 June 2022
Available online 18 June 2022

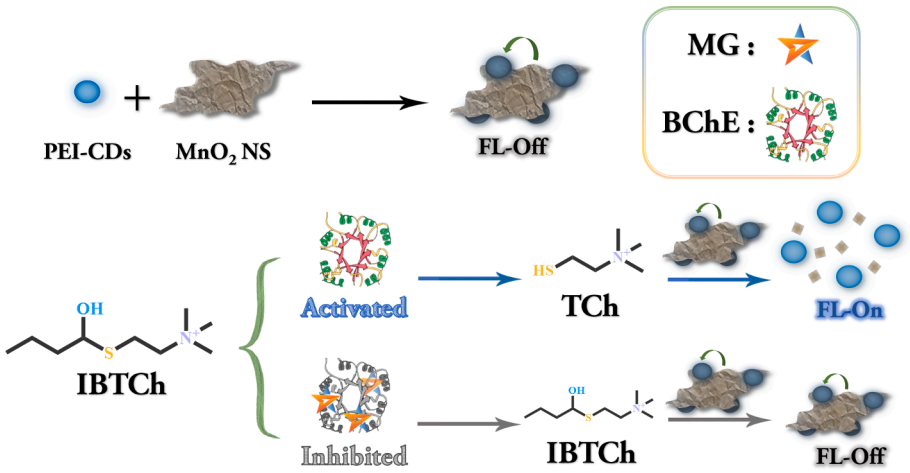

Scheme 1. Schematic diagram of the developed sensing strategy based on BPEI-CDs and MnO_2 NS for MG determination.

2017), and colorimetry (Shi, Zhang, Yu, Liu, & Chen, 2019). Although the response speed of SERS and electrochemical analysis is not slow, electrochemical analysis requires repeated calibration of electrodes, and SERS is susceptible to substrate interference. In addition, HPLC and ELISA require cumbersome and complicated instrument operations, and colorimetric methods have low sensitivity and poor selectivity. In comparison, fluorescence spectroscopy has simpler instrument operation, inexpensive equipment, second only to UV–visible spectrophotometer in popularity, and the detection method is more conducive to popularization (Han, Kong, Hou, Chen, Zhang, & Zheng, 2020; Li, Lin, Chen, Zhang, Lin, Lai, et al., 2015; Le Wu, Lin, Zhong, Chen, & Huang, 2017). To date, sensors based on the fluorescence method have exhibited significant advantages over other methods, including rapid analysis times, high sensitivity and easy operation (Hiremath, Bhosle, Nayse, Biswas, Biswas, Bhasikuttan, et al., 2021; Zhu, Yuan, Han, Liu, & Sun, 2021).

Among the developed fluorescent materials, carbon dots (CDs) have attracted increasing attention for various applications due to their high solubility, low toxicity, good biocompatibility, highly stable fluorescence and relatively low-cost (Wang, Wang, Cheng, Geng, Wang, Dong, et al., 2021; Yoo, Kwak, & Kim, 2021). The excellent fluorescence characteristics of CDs have resulted in their application in various fields such as bioimaging (Zhang & Yu, 2016), drug delivery (Peng, Han, Li, Al-Youbi, Bashammakh, El-Shahawi, et al., 2017) and catalysis (Hutton, Martindale, & Reisner, 2017).

Manganese dioxide nanosheets (MnO_2 NS) is a 2D material with a broad absorption band that is degradable and easily modified (Chen, Meng, Tian, Yang, Du, Li, et al., 2019). MnO_2 NS have exhibited good prospects for use in various fluorescent sensing platforms and biomedical applications, due to their excellent light absorption properties and large surface area (Li, Zhang, Zhang, Liu, Chen, Liu, et al., 2021; Liu, Liu, & Zhou, 2019). To date, combinations of fluorescent probes and nanomaterial-based quenchers (such as MnO_2 NS, gold nanoparticles (AuNPs), graphene oxide (GO) (Cheng, Cen, Xu, Wei, Shi, Xu, et al., 2018; Dehghani, Mohammadnejad, Hosseini, bakhshi, & Rezayan, 2020), and Fe_3O_4 nanoplates (Chen, Rong, Cen, Xu, Xie, Yang, et al., 2021) have been effectively applied in the design of promising novel sensors (Qaddare & Salimi, 2017).

Förster resonance energy transfer (FRET) refers to the process of transferring energy from the donor to the acceptor through nonradiative dipole–dipole coupling after the donor transitions from the ground state to the excited state. FRET occurs when the distance between the donor (fluorescence emitter) and acceptor (absorber) is in the nanometer (~10 nm) range and when the emission spectrum of the donor overlaps with the absorption spectrum of the acceptor, energy can be transferred nonradiatively. Due to the well overlapping between the absorption band of MnO_2 NS and the fluorescence emission (445 nm) of BPEI-CDs, MnO_2 NS could serve as a fluorescence quencher to effectively quench the fluorescence of BPEI-CDs.

Herein, BPEI-CDs and MnO_2 NS were synthesized using a simple one-step, low-temperature process and a facile fluorescence system was developed for the sensitive detection of MG. As illustrated in Scheme 1, MnO_2 NS quenches the fluorescence of BPEI-CDs at 445 nm via FRET. Butyrylcholinesterase (BChE) was used to generate thiocholine from the substrate S-butyrylthiocholine iodide (IBTCh), with thiocholine effectively decomposing MnO_2 NS to Mn^{2+}, thereby restoring the fluorescence of BPEI-CDs. As an enzyme inhibitor of BChE activity, MG can prevent the production of thiocholine and inhibit the decomposition of MnO_2 NS, causing an inhibition of fluorescence in the system.

2. Experimental section

2.1. Chemicals and materials

Citric acid (CA), sodium dodecyl sulfate (SDS), and S-Butyrylthiocholine iodide (IBTCh) were purchased from J&K Chemical Technology Company Ltd (Beijing, China). Branched poly(ethylenimine) (BPEI, M = 1800) and ammonium acetate were acquired from Aladdin Industrial Company Ltd (Shanghai, China). Butyrylcholinesterase (BChE) was purchased from Shanghai Yuanye Biotechnology Company Ltd (China). Malachite green was acquired from Alta Scientific Company Ltd (Tianjin, China). Potassium permanganate ($KMnO_4$) was purchased from Tianjin Chemical Reagent Company Ltd (China). HPLC-grade acetonitrile was purchased from Fisher Scientific Company (Pittsburgh, USA). Deionized water (18.2 MΩ cm) was used throughout the analyses and Tris-HCl buffer (12.5 mM, pH = 8) was prepared for further use.

2.2. Apparatus

Fluorescence spectra were recorded on a F-2700 Spectro fluorophotometer (HITACHI Co., Ltd., Japan) with excitation slits and emission slits of 10 nm and a PMT Voltage of 400 V. Absorption spectra were recorded on a Cary 60 UV–vis spectrometer (Agilent Technologies Inc., USA). FT-IR spectra were investigated using KBr pellets on a Nicolet Avatar360 FT-IR spectrophotometer (Thermo Fisher Scientific Inc., USA) in the range of 4000–400 cm^{-1}. TEM images were conducted on a JEM-2100F Transmission Electron Microscope (JEOL, Japan). XPS was conducted on the ESCALAB 250 spectrometer (Thermo Fisher Scientific Inc., USA). Fluorescence lifetime was obtained on the FLS920 spectrometer (Edinburgh Instrument, UK). All pH values were measured with a PHS-3C pH-Meter (INESA Scientific Inc., China). Fish samples were determined with a Shimadzu LC-20ADXR liquid chromatograph

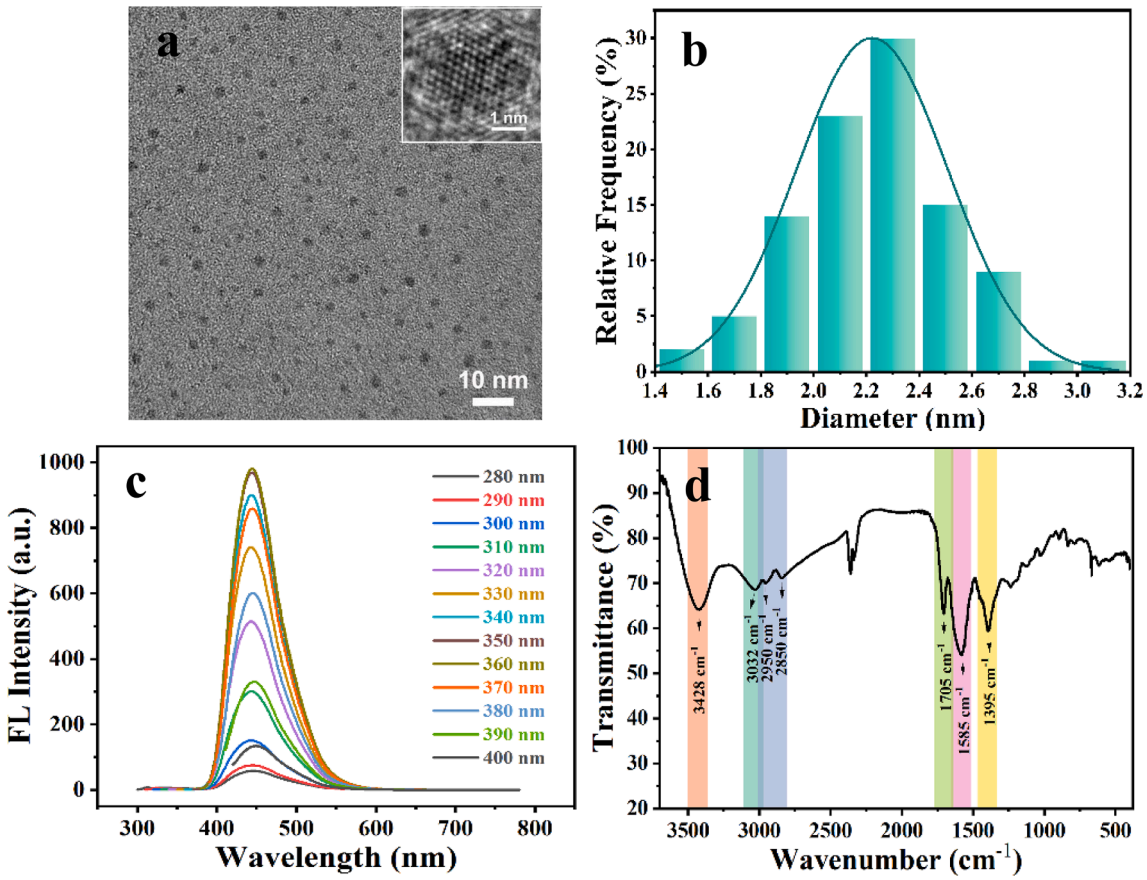

Fig. 1. (a) TEM image of the BPEI-CDs; (b) Size distribution of the BPEI-CDs; (c) Fluorescence emission spectra of the BPEI-CDs at various excitation wavelengths (280–400 nm); (d) FT-IR spectra of the BPEI-CDs.

system (Shimadzu, Japan).

2.3. Synthesis of BPEI-CDs

BPEI-CDs with a high quantum yield (exceeding 40%) were synthesized according to a previously reported method with some modifications (Dong, Wang, Li, Shao, Chi, Lin, et al., 2012). Briefly, BPEI (0.5 g) and CA (1.0 g) were dissolved in 10 mL water in a 50 mL beaker by heating to 160 °C using a heating plate. After boiled, the solution temperature was then reduced to 135 °C. As most of the water evaporated, a pale-yellow gel was obtained. Then, 1 mL of water was added to rehydrate the gel and avoid scorching. The same procedure was repeated more than 10 times until the color of the gel turned orange, indicating the successful formation of BPEI-CDs. Next, deionized water was immediately added to adjust the solution volume to 10 mL and the mixture was shaken until the gel was fully dissolved. The resulting BPEI-CDs solution was stored in the dark at 4 °C prior to use.

2.4. Synthesis of MnO_2 NS

The procedure for MnO_2 NS synthesis was performed according to a previously reported method as follows (Wei, Cui, Chen, & Ivey, 2011): First, 10 mL of 0.1 mol/L sodium dodecyl sulfate solution and 0.5 mL of 0.1 mol/L H_2SO_4 solution were dispersed in 88.5 mL of deionized water and heated at 95 °C for 15 min. Then, 1 mL of 0.05 mol/L $KMnO_4$ solution was slowly added to the mixture and heated for another 60 min. The as-synthesized MnO_2 NS were then cooled to ambient temperature and washed three times with deionized water. Finally, MnO_2 NS were vacuum-dried, forming dark-brown solid flakes.

2.5. Quenching of BPEI-CDs by MnO_2 NS

Varying volumes of 2 mg/mL MnO_2 NS solution were added to 10 μL of 10.4 mg/mL BPEI-CDs, with the mixture then diluted using Tris-HCl (12.5 mM, pH 8) to a final volume of 500 μL. The mixture was then incubated for 2 min prior to fluorescence emission spectra measurements.

2.6. Detection procedure for BChE

First, different concentration BChE (20 μL) solutions were mixed with 50 μL of IBTCh (10 mM) and 40 μL of Tris-HCl (12.5 mM, pH 8), then incubated for 30 min at 37 °C. Then, 300 μL of MnO_2 NS (2 mg/mL) were added to the mixture and incubated for 30 min. Following this, 10 μL of BPEI-CDs (10.4 mg/mL) were added, and the mixtures were diluted to 500 μL with deionized water and thoroughly mixed. Finally, the fluorescence emission spectra were recorded.

2.7. Procedure for MG detection

For the detection of MG, 20 μL of varying concentration MG solutions and 20 μL of BChE (3×10^3 U/L) were mixed with 40 μL Tris-HCl (12.5 mM, pH 8) at 37 °C for 30 min. Then, 50 μL of IBTCh (10 mM) was added and the mixture was incubated at 37 °C for 20 min. Next, 300 μL of MnO_2 NS (2 mg/mL) were added and after 2 min of incubation, and 10 μL of BPEI-CDs (10.4 mg/mL) were added and the mixtures were diluted to 500 μL with deionized water. Finally, fluorescence emission spectra detection was performed at an excitation wavelength of 360 nm.

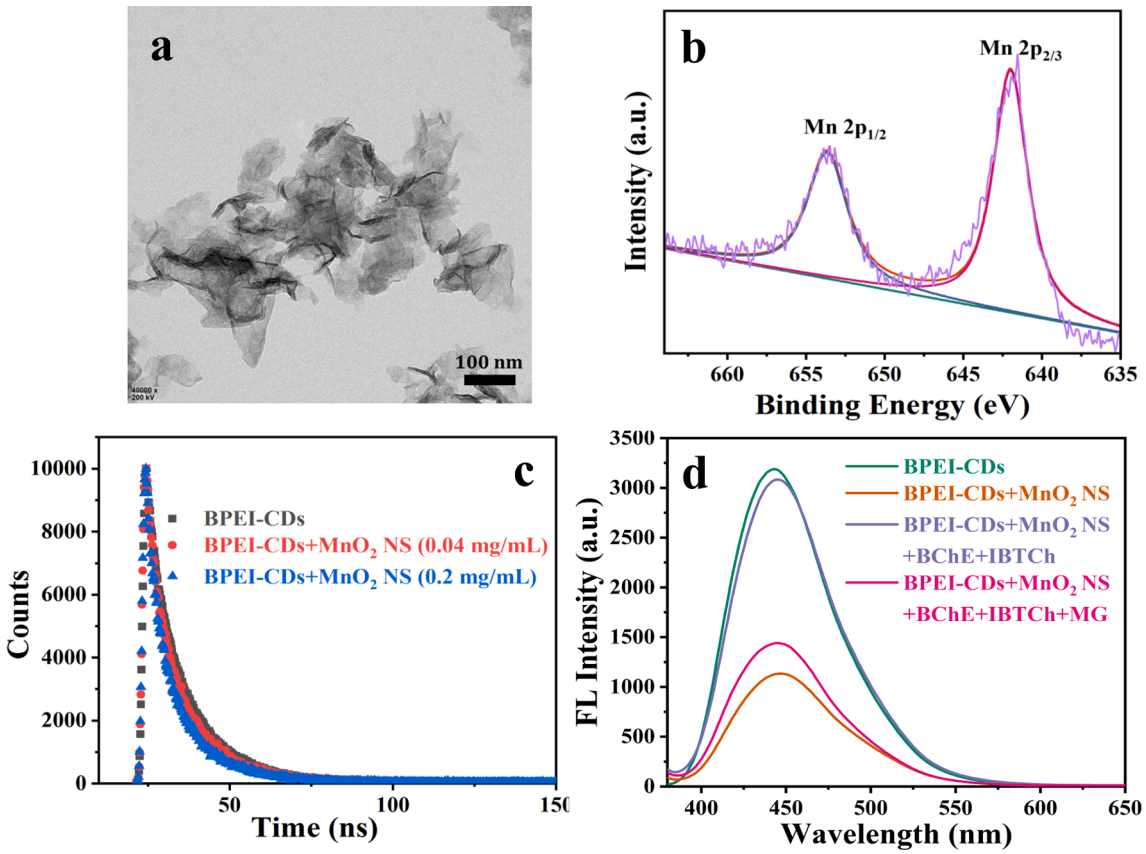

Fig. 2. (a) TEM image of MnO_2 NS; (b) High resolution XPS spectra of Mn 2p. (c) Fluorescence lifetimes of BPEI-CDs (0.52 mg/mL); (d) The change in fluorescence spectra of BPEI-CDs upon the addition of a diverse range of reaction components. 0.208 mg/mL BPEI-CDs; 1.2 mg/mL MnO_2 NS; 120 U/L BChE; 1 mM IBTCh; 10 μM MG.

2.8. Determination of MG in fish tissue samples

The standard addition method was used to establish the MG content in fish tissue. Deceased bluntnose black bream was purchased from a local supermarket in Changchun, China. After removing the scales and skin from the fish, the tissue along the back of the fish was collected and homogenized into a paste. 4 g of fish paste per sample was combined with 10 mL of acetonitrile and ultrasonicated for 10 min. The mixture was centrifuged at 6000 rpm for 5 min and the supernatant was transferred to a centrifuge tube. The precipitate was extracted again using the same method and the two supernatants were then combined and evaporated in a nitrogen atmosphere. Subsequently, the residue was dissolved using Tris-HCl solution to 10 mL and filtered through a 0.22 μm membrane. For each processed fish sample, 50 μL was combined with different MG samples, using the constructed method to detect the MG concentration and calculate the recovery rate accordingly. The determination method of HPLC refers to the National Standard of the P.R.C GB/T 19857–2005 (Residues of Malachite Green and Crystal Violet in Aquatic Products). The chromatographic separation was performed on an eclipse XDB-C18 column (150 mm × 4.6 mm, 5.0 μm particle size) with a mobile phase consisting of ammonium acetate (50 mmol·L^{-1}, pH 4.5) -acetonitrile (40:60, v/v) at a flow rate of 1.0 mL min^{-1}. Detection wavelength and sample injection volume were 618 nm and 50 μL, respectively.

3. Results and discussion

3.1. Characterization of BPEI-CDs

The BPEI-CDs were synthesized via a simple one-step low-temperature pyrolysis method using CA and BPEI as precursors. Transmission electron microscope (TEM) imaging confirmed that BPEI-CDs were spherical and well dispersed in aqueous solution, with an average diameter of 2.3 nm (Fig. 1a & 1b). The high-resolution TEM images (inset of Fig. 1a) revealed that the BPEI-CDs exhibited a lattice spacing distance of 0.21 nm, corresponding to graphite (1 0 0) (Dong, et al., 2012). As shown in Fig. 1c, when the excitation wavelength was changed from 280 to 400 nm, the BPEI-CDs solution exhibited a fluorescence emission peak at 445 nm. Therefore, considering the fluorescence intensity at different emission wavelengths, 360 nm was selected as the excitation wavelength for all following experiments.

FT-IR spectrum analysis was used to characterize the surface functional groups of BPEI-CDs. As shown in Fig. 1d, the strong absorption bands at 3428 cm^{-1} and 1585 cm^{-1} were assigned to the stretching vibrations of N—H, while the weak absorption bands at 2950 and 2850 cm^{-1} were attributed to C—H stretching vibrations. Furthermore, the absorption bands at 1395 cm^{-1} and 1705 cm^{-1} were assigned to the stretching vibrations of C — N and C═O, respectively, while a sharp peak at 1705 cm^{-1} corresponded to – CONH–, which is formed by the dehydration condensation of $–NH_2$ groups from BPEI and the –COOH groups of carbonized CA (J.-Y. Li, Liu, Shu, Liang, Zhang, Chen, et al., 2017).

The UV–vis absorption spectra of the as-prepared BPEI-CDs exhibited two distinct absorption bands at 245 and 360 nm, which were ascribed to the π–π* transition of the aromatic ring and n–π* transition of C═O, respectively (Fig. S1). A xenon lamp was used to test the photostability of BPEI-CDs under continuous intensive excitation conditions. As shown in Fig. S2, it was observed that the normalized fluorescence emission intensity of BPEI-CDs remained at the same intensity level after 60 min of xenon lamp irradiation, indicating that CDs exhibited good

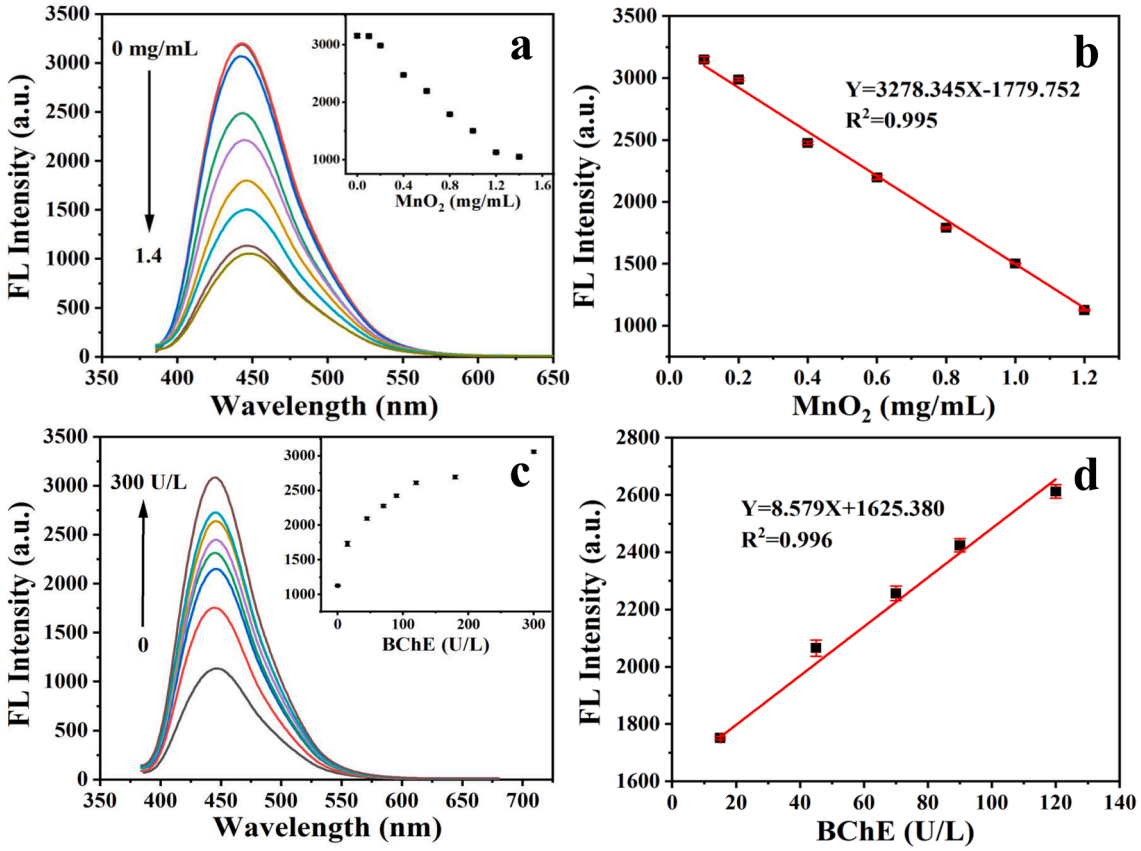

Fig. 3. (a) Fluorescence spectra of BPEI-CDs in the presence of varying concentrations of MnO_2 NS (0, 0.1, 0.2, 0.3, 0.4, 0.6, 0.8, 1.0, 1.2, or 1.4 mg/mL); (b) The linear plot of fluorescence intensity of BPEI-CDs with varying concentrations of MnO_2 NS. (c) Fluorescence spectra of the BPEI-CDs-MnO_2 NS-BChE-IBTCh system in the presence of varying concentrations of BChE (0, 15, 45, 70, 90, 120, 180, or 300 U/L); (d) Linear plot of the fluorescence intensity of the BPEI-CDs-MnO_2 NS-BChE-IBTCh system with varying concentrations of BChE.

photostability. The fluorescence response of BPEI-CDs was found to be pH-dependent within the pH range from 5 − 10, with BPEI-CDs exhibiting strong fluorescence and a maximum response at pH 6 significantly decreasing under increasing pH conditions (Fig. S3).

3.2. Design of the BPEI-CDs and MnO_2 NS system

TEM and XPS spectra were used to characterize the MnO_2 NS prepared using a redox reaction between SDS and $KMnO_4$. TEM image confirmed our successful synthesis of MnO_2 NS. As shown in Fig. 2a, the TEM image revealed that the MnO_2 NS displayed a thin and irregular two-dimensional sheet-like structure, containing fine wrinkles which provide sufficient surface coverage for the fixation of BPEI-CDs. (See Fig. 3).

Fig. 2b displays Mn 2p in the high-resolution XPS spectrum for MnO_2 NS, with the peaks at 642.0 eV and 653.6 eV assigned to Mn $2p_{3/2}$ and Mn $2p_{1/2}$, respectively. These characterization results confirmed the successful preparation of MnO_2 NS. Furthermore, MnO_2 NS have a broad UV − vis absorption spectrum range (250 nm–800 nm) and a peak centered at 385 nm, with a significant overlap area between the emission peak of BPEI-CDs and MnO_2 NS absorption (Fig. S4). The broad absorption peak could make MnO_2 NS a feasible energy acceptor for BPEI-CDs. In addition, the absorption spectra of MnO_2 NS and the BPEI-CDs mixture exhibited a blue shift compared to that of MnO_2 NS, due to the electrostatic interaction between MnO_2 NS and BPEI-CDs (Fig. S5).

Furthermore, the zeta potential of BPEI-CDs was positively charged ($\zeta = +8.29$ mV), while for MnO_2 NS it was negatively charged ($\zeta = -3.98$ mV). The mixture of BPEI-CDs and MnO_2 NS resulted in a zeta potential of + 2.39 mV (Fig. S6). Therefore, electrostatic interactions between the BPEI-CDs and MnO_2 NS could bring them closer, meeting the donor–acceptor distance requirements for FRET.

The fluorescence lifetime of BPEI-CDs in the presence of different concentrations of MnO_2 NS were studied (Fig. 2c). The double exponential function was used to fit the fluorescence decay curve, establishing a lifetime for BPEI-CDs of 12.12 ns. With increasing MnO_2 NS concentrations from 0.04 to 0.2 mg/mL, the fluorescence lifetimes gradually decreased from 11.42 to 10.56 ns, implying that BPEI-CDs could be applied as an energy donor and that MnO_2 NS served as a nano-quencher and energy acceptor through FRET.

3.3. Feasibility of this method and mechanism of function

The feasibility of sensing MG using this novel method is presented in Fig. 2d. Specifically, the fluorescence of BPEI-CDs at 445 nm can be quenched by MnO_2 NS. After the addition of BChE and IBTCh, fluorescence was restored to about 96.6% of the original level. However, the addition of MG led to a decrease in the fluorescence intensity of BPEI-CDs at an excitation wavelength of 360 nm. Furthermore, the BPEI-CDs were separately incubated with BChE, IBTCh and MG under the same conditions, resulting in no significant effect on the fluorescence of BPEI-CDs (Fig. S7). These results demonstrate that this method is both feasible and practical for the detection of MG.

3.4. Optimization of detection conditions

To establish the optimal conditions for MG detection, the fluorescence spectra were recorded at different concentrations of MnO_2 NS, BChE, and IBTCh. In addition, the effects of varying pH levels and

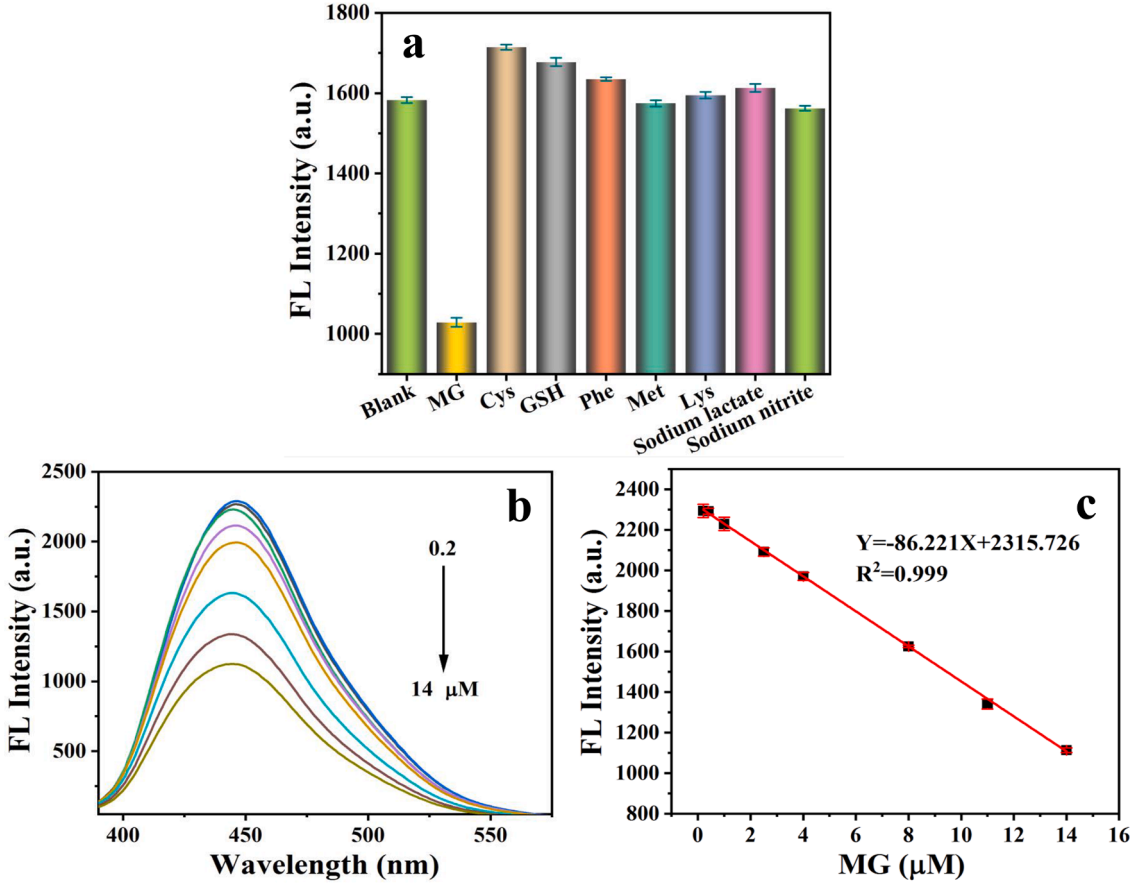

Fig. 4. (a)Fluorescence intensity of the sensing system with the addition of MG (10 μM) and interfering substances (100 μM). (b) The fluorescence spectra of the BPEI-CDs-MnO_2 NS-BChE-IBTCh system in the presence of varying concentrations of MG (0.2, 0.4, 1, 2.5, 4, 8, 11, or 14 μM); (c) Linear plot of the FL intensity of the BPEI-CDs-MnO_2 NS-BChE-IBTCh system versus MG concentration.

enzyme reaction times on the system were also recorded, while 37 ℃ was maintained as the constant temperature for the catalytic reaction of BChE.

As exhibited in Fig. 4a, the MnO_2 NS fluorescence quenching responses of BPEI-CDs were explored. The fluorescence intensity of BPEI-CDs decreased gradually with increasing concentrations of MnO_2 NS from 0 to 1.4 mg/mL, with the fluorescence quenching efficiency reaching 64% after incubation with 1.2 mg/mL MnO_2 NS. Fig. 4b shows the linear plot of fluorescence intensity and MnO_2 NS concentration from 0.1 to 1.2 mg/mL, with a linear regression equation of $Y = 3278.345X-1779.752$ ($R^2 = 0.995$). Therefore, 1.2 mg/mL was selected as the MnO_2 NS concentration for all subsequent experiments.

Fig. 4c exhibits gradual increase in the fluorescence intensity of the sensing system with increasing levels of BChE. As shown in Fig. 4d a good linear relationship was observed between the fluorescence intensity of the BPEI-CDs-MnO_2 NS-BChE-IBTCh system and BChE concentration, with the linear regression equation $Y = 8.579X + 1625.380$ ($R^2 = 0.996$) obtained in the range of 15–120 U/L. Accordingly, 120 U/L was selected as the optimal concentration of BChE.

The pH and enzyme reaction time impact of the sensing system was also investigated (Fig. S8), with results indicating that the fluorescence intensity reached a maximum at pH 8. The effect of reaction time (over a 0–40 min range) at 37 °C on the fluorescence intensity of the system is shown in Fig. S8, indicating that the enzymatic reaction reached equilibrium at 40 min. Therefore, pH 8 was selected as the optimal pH level and the enzyme reaction time was set to 40 min for MG detection.

3.5. System selectivity

The selectivity of the system was evaluated by parallel measurement of the fluorescence response to certain biomolecules (Cys, GSH, Phe, Met, and Lys) and preservatives (sodium lactate and sodium nitrite). As shown in Fig. 4a, the MG sensing system exhibited high specificity against other interfering substances, enhance its application in the analysis of complex biological samples.

Table 1
Recovery tests of spiked MG in fish samples measured with our method and HPLC, respectively ($n = 3$).

Spiked MG (μM)	Our method			HPLC			δ Relative Error (%)
	Found (μM)	Recovery (%)	RSD (%)	Found (μM)	Recovery (%)	RSD (%)	
0	ND	–	–	ND	–	–	–
1	1.02	101.71	8.65	0.95	95.16	3.68	7.00
3	3.24	108.28	6.42	3.07	102.25	5.23	5.67
7	6.97	99.58	1.16	7.24	103.49	7.59	3.86
10	10.09	100.90	0.94	11.13	111.34	7.28	10.40

3.6. Quantitative determination of MG

Under optimal conditions, the linear relationship and detection limit of the sensing system were established. As presented in Fig. 4b and Fig. 4c, with increasing concentrations of MG, the fluorescence intensity was gradually quenched. A good linear relationship ($R^2 = 0.999$) was obtained in the range of 0.2 to 14 μM MG (regression equation of Y = -86.221X + 2315.726), with the detection limit for MG calculated to be 0.06 μM (signal-to-noise ratio of 3).

3.7. Real sample detection

The high sensitivity and selectivity of the proposed sensing system make it a promising candidate for the detection of MG in real samples. Diluted fish tissue samples spiked with a series of known MG concentrations were examined. The developed methods have been validated by HPLC method according to the National Standard of the P.R.C GB/T 19857–2005. Based on the results listed in Table 1, the developed method showed satisfactory recoveries ranging from average MG recoveries ranged from 99.58% to 108.28% with relative standard deviation (RSD) below 8.65%. Besides, the recovery for determination of MG by HPLC ranged from 95.16% to 111.34% with a low RSD of 3.68%–7.59%. The relative errors (δ) of the detection results obtained using our method and those obtained using HPLC ranged from 3.9% to 10.4%, which indicating the high accuracy and potential applicability of the proposed sensor for MG analysis in fish tissue samples.

4. Conclusions

In this study, a simple and sensitive assay for MG detection was developed based on the FRET between BPEI-CDs and MnO_2 NS. BPEI-CDs were used as a fluorophore and MnO_2 NS served as a fluorescence quencher and recognized the substrate. The linear relationship between MG concentrations and fluorescence signal reduction was established and used for the quantitative analysis of MG concentration within the range of 0.2 to 14 μM, with a detection limit of 0.06 μM. Furthermore, this novel method achieved excellent spiked sample recoveries, serving as a promising system for the rapid and accurate detection of MG.

CRediT authorship contribution statement

Xiaowei Mu: Conceptualization, Methodology, Investigation, Formal analysis, Writing – original draft. **Xin Liu:** Data curation, Visualization. **Xiwen Ye:** Resources, Validation. **Wei Zhang:** Resources, Investigation. **Lu Li:** Writing – review & editing, Resources. **Pinyi Ma:** Writing – review & editing, Supervision, Project administration. **Daqian Song:** Funding acquisition, Project administration.

Declaration of Competing Interest

The authors declare that they have no known competing financial interests or personal relationships that could have appeared to influence the work reported in this paper.

Acknowledgments

This work was supported by the National Natural Science Foundation of China (Grant nos. 22004052 and 22074046), Capital Construction Funds within the Jilin Provincial Budget (2020C022-8).

Appendix A. Supplementary data

Supplementary data to this article can be found online at https://doi.org/10.1016/j.foodchem.2022.133517.

References

Alderman, D. J. (1985). Malachite green: A review. *Journal of Fish Diseases, 8*(3), 289–298.
Aydin, F., Yilmaz, E., & Soylak, M. (2017). A simple and novel deep eutectic solvent based ultrasound-assisted emulsification liquid phase microextraction method for malachite green in farmed and ornamental aquarium fish water samples. *Microchemical Journal, 132*, 280–285.
Chen, J., Meng, H., Tian, Y., Yang, R., Du, D., Li, Z., … Lin, Y. (2019). Recent advances in functionalized MnO2 nanosheets for biosensing and biomedicine applications. *Nanoscale Horizons, 4*(2), 321–338.
Chen, Q., Rong, S., Cen, Y., Xu, G., Xie, Z., Yang, J., … Wei, F. (2021). A facile fluorescent sensor based on carbon dots and Fe_3O_4 nanoplates for the detection of hyaluronidase activity. *Sensors and Actuators B: Chemical, 346*, Article 130434.
Cheng, X., Cen, Y., Xu, G., Wei, F., Shi, M., Xu, X., … Hu, Q. (2018). Aptamer based fluorometric determination of ATP by exploiting the FRET between carbon dots and graphene oxide. *Microchimica Acta, 185*(2), 144.
da Cunha, D. T. (2021). Improving food safety practices in the foodservice industry. *Current Opinion in Food Science, 42*, 127–133.
Dehghani, Z., Mohammadnejad, J., Hosseini, M., Bakhshi, B., & Rezayan, A. H. (2020). Whole cell FRET immunosensor based on graphene oxide and graphene dot for Campylobacter jejuni detection. *Food Chemistry, 309*, Article 125690.
Deng, D., Lin, Q., Li, H., Huang, Z., Kuang, Y., Chen, H., & Kong, J. (2019). Rapid detection of malachite green residues in fish using a surface-enhanced Raman scattering-active glass fiber paper prepared by in situ reduction method. *Talanta, 200*, 272–278.
Dong, Y., Wang, R., Li, H., Shao, J., Chi, Y., Lin, X., & Chen, G. (2012). Polyamine-functionalized carbon quantum dots for chemical sensing. *Carbon, 50*(8), 2810–2815.
Fallah, A. A., & Barani, A. (2014). Determination of malachite green residues in farmed rainbow trout in Iran. *Food Control, 40*, 100–105.
Foster, F. J., & Woodbury, L. (1936). The Use of Malachite Green as a Fish Fungicide and Antiseptic. *The Progressive Fish-Culturist, 3*(18), 7–9.
Gavrilenko, N. A., Volgina, T. N., Pugachev, E. V., & Gavrilenko, M. A. (2019). Visual determination of malachite green in sea fish samples. *Food Chemistry, 274*, 242–245.
Han, L.-J., Kong, Y.-J., Hou, G.-Z., Chen, H.-C., Zhang, X.-M., & Zheng, H.-G. (2020). A Europium-based MOF Fluorescent Probe for Efficiently Detecting Malachite Green and Uric Acid. *Inorganic Chemistry, 59*(10), 7181–7187.
Hiremath, S. D., Bhosle, A. A., Nayse, A., Biswas, S., Biswas, M., Bhasikuttan, A. C., … Chatterjee, A. (2021). A redox-coupled carbon dots-MnO_2 nanosheets based sensory platform for label-free and sensitive detection of E. coli. *Sensors and Actuators B: Chemical, 339*, Article 129918.
Hutton, G. A. M., Martindale, B. C. M., & Reisner, E. (2017). Carbon dots as photosensitisers for solar-driven catalysis. *Chemical Society Reviews, 46*(20), 6111–6123.
Jiang, Y., Xie, P., & Liang, G. (2009). Distribution and depuration of the potentially carcinogenic malachite green in tissues of three freshwater farmed Chinese fish with different food habits. *Aquaculture, 288*(1), 1–6.
Khan, M. A., Otero, M., Kazi, M., Alqadami, A. A., Wabaidur, S. M., Siddiqui, M. R., … Sumbul, S. (2019). Unary and binary adsorption studies of lead and malachite green onto a nanomagnetic copper ferrite/drumstick pod biomass composite. *Journal of Hazardous Materials, 365*, 759–770.
Leteux, F., & Meyer, F. P. (1972). Mixtures of Malachite Green and Formalin for Controlling Ichthyophthirius and other Protozoan Parasites of Fish. *The Progressive Fish-Culturist, 34*(1), 21–26.
Li, J.-Y., Liu, Y., Shu, Q.-W., Liang, J.-M., Zhang, F., Chen, X.-P., … Tan, K.-J. (2017). One-Pot Hydrothermal Synthesis of Carbon Dots with Efficient Up- and Down-Converted Photoluminescence for the Sensitive Detection of Morin in a Dual-Readout Assay. *Langmuir, 33*(4), 1043–1050.
Li, L., Lin, Z.-Z., Chen, X.-M., Zhang, H.-Y., Lin, Y.-D., Lai, Z.-Z., & Huang, Z.-Y. (2015). Molecularly imprinted polymers for extraction of malachite green from fish samples prior to its determination by HPLC. *Microchimica Acta, 182*(9), 1791–1796.
Li, L., Peng, A.-H., Lin, Z.-Z., Zhong, H.-P., Chen, X.-M., & Huang, Z.-Y. (2017). Biomimetic ELISA detection of malachite green based on molecularly imprinted polymer film. *Food Chemistry, 229*, 403–408.
Li, Y.-H., Yang, T., Qi, X.-L., Qiao, Y.-W., & Deng, A.-P. (2008). Development of a group selective molecularly imprinted polymers based solid phase extraction of malachite green from fish water and fish feed samples. *Analytica Chimica Acta, 624*(2), 317–325.
Li, Y., Zhang, L., Zhang, Z., Liu, Y., Chen, J., Liu, J., … Lu, X. (2021). MnO2 Nanospheres Assisted by Cysteine Combined with MnO_2 Nanosheets as a Fluorescence Resonance Energy Transfer System for "Switch-on" Detection of Glutathione. *Analytical Chemistry, 93*(27), 9621–9627.
Liu, J., Liu, C., & Zhou, Z. (2019). A turn-on fluorescent sulfide probe prepared from carbon dots and MnO_2 nanosheets. *Microchimica Acta, 186*(5), 281.
Mittelstaedt, R. A., Mei, N., Webb, P. J., Shaddock, J. G., Dobrovolsky, V. N., McGarrity, L. J., … Heflich, R. H. (2004). Genotoxicity of malachite green and leucomalachite green in female Big Blue $B_6C_3F_1$ mice. *Mutation Research/Genetic Toxicology and Environmental Mutagenesis, 561*(1), 127–138.
Nyarugwe, S. P., Linnemann, A., Hofstede, G. J., Fogliano, V., & Luning, P. A. (2016). Determinants for conducting food safety culture research. *Trends in Food Science & Technology, 56*, 77–87.
Peng, Z., Han, X., Li, S., Al-Youbi, A. O., Bashammakh, A. S., El-Shahawi, M. S., & Leblanc, R. M. (2017). Carbon dots: Biomacromolecule interaction, bioimaging and nanomedicine. *Coordination Chemistry Reviews, 343*, 256–277.

Qaddare, S. H., & Salimi, A. (2017). Amplified fluorescent sensing of DNA using luminescent carbon dots and AuNPs/GO as a sensing platform: A novel coupling of FRET and DNA hybridization for homogeneous HIV-1 gene detection at femtomolar level. *Biosensors and Bioelectronics, 89*, 773–780.

Sacara, A. M., Cristea, C., & Muresan, L. M. (2017). Electrochemical detection of Malachite Green using glassy carbon electrodes modified with CeO_2 nanoparticles and Nafion. *Journal of Electroanalytical Chemistry, 792*, 23–30.

Samiey, B., & Toosi, A. R. (2010). Adsorption of malachite green on silica gel: Effects of NaCl, pH and 2-propanol. *Journal of Hazardous Materials, 184*(1), 739–745.

Shi, H., Zhang, L., Yu, G., Liu, Y., & Chen, L. (2019). Molecularly imprinted mesoporous silica incorporating C_3N_4 dots and CdTe quantum dots as ratiometric fluorescent probe for determination of Malachite Green. *Microchimica Acta, 186*(8), 556.

Srivastava, S., Sinha, R., & Roy, D. (2004). Toxicological effects of malachite green. *Aquatic Toxicology, 66*(3), 319–329.

Stammati, A., Nebbia, C., Angelis, I. D., Albo, A. G., Carletti, M., Rebecchi, C., … Dacasto, M. (2005). Effects of malachite green (MG) and its major metabolite, leucomalachite green (LMG), in two human cell lines. *Toxicology in Vitro, 19*(7), 853–858.

Wang, Z., Wang, H., Cheng, X., Geng, J., Wang, L., Dong, Q., … Chi, Z. (2021). Aptamer-superparamagnetic nanoparticles capture coupling siderophore-Fe^{3+} scavenging actuated with carbon dots to confer an "off-on" mechanism for the ultrasensitive detection of Helicobacter pylori. *Biosensors and Bioelectronics, 193*, Article 113551.

Wei, W., Cui, X., Chen, W., & Ivey, D. G. (2011). Manganese oxide-based materials as electrochemical supercapacitor electrodes. *Chemical Society Reviews, 40*(3), 1697–1721.

Wu, L., Lin, Z.-Z., Zhong, H.-P., Chen, X.-M., & Huang, Z.-Y. (2017). Rapid determination of malachite green in water and fish using a fluorescent probe based on CdTe quantum dots coated with molecularly imprinted polymer. *Sensors and Actuators B: Chemical, 239*, 69–75.

Wu, L., Xu, Z., Meng, Q., Xiao, Y., Cao, Q., Rathi, B., … Yan, J. (2020). A new aptamer/black phosphorous interdigital electrode for malachite green detection. *Analytica Chimica Acta, 1099*, 39–45.

Xie, J., Peng, T., Chen, D.-D., Zhang, Q.-J., Wang, G.-M., Wang, X., … Deng, J. (2013). Determination of malachite green, crystal violet and their leuco-metabolites in fish by HPLC–VIS detection after immunoaffinity column clean-up. *Journal of Chromatography B, 913–914*, 123–128.

Xu, K.-X., Guo, M.-H., Huang, Y.-P., Li, X.-D., & Sun, J.-J. (2018). Rapid and sensitive detection of malachite green in aquaculture water by electrochemical preconcentration and surface-enhanced Raman scattering. *Talanta, 180*, 383–388.

Yoo, H. J., Kwak, B. E., & Kim, D. H. (2021). Competition of the roles of π-conjugated domain between emission center and quenching origin in the photoluminescence of carbon dots depending on the interparticle separation. *Carbon, 183*, 560–570.

Zhang, J., & Yu, S.-H. (2016). Carbon dots: Large-scale synthesis, sensing and bioimaging. *Materials Today, 19*(7), 382–393.

Zhou, X., Zhang, J., Pan, Z., & Li, D. (2019). Review of Methods for the Detection and Determination of Malachite Green and Leuco-Malachite Green in Aquaculture. *Critical Reviews in Analytical Chemistry, 49*(1), 1–20.

Zhu, X., Yuan, X., Han, L., Liu, H., & Sun, B. (2021). A smartphone-integrated optosensing platform based on red-emission carbon dots for real-time detection of pyrethroids. *Biosensors and Bioelectronics, 191*, Article 113460.